Structural insights into α-synuclein monomer–fibril interactions

Pratibha Kumari[a,1], Dhiman Ghosh[a,1], Agathe Vanas[a], Yanick Fleischmann[a], Thomas Wiegand[a], Gunnar Jeschke[a], Roland Riek[a,2], and Cédric Eichmann[a,b,2]

[a]Department of Chemistry and Applied Biosciences, Laboratory of Physical Chemistry, ETH Zurich, 8093 Zurich, Switzerland; and [b]Department of Biological Regulation, Weizmann Institute of Science, 76100 Rehovot, Israel

Edited by Robert Tycko, National Institute of Diabetes and Digestive and Kidney Diseases, Bethesda, MD, and approved January 12, 2021 (received for review June 12, 2020)

Protein aggregation into amyloid fibrils is associated with multiple neurodegenerative diseases, including Parkinson's disease. Kinetic data and biophysical characterization have shown that the secondary nucleation pathway highly accelerates aggregation via the absorption of monomeric protein on the surface of amyloid fibrils. Here, we used NMR and electron paramagnetic resonance spectroscopy to investigate the interaction of monomeric α-synuclein (α-Syn) with its fibrillar form. We demonstrate that α-Syn monomers interact transiently via their positively charged N terminus with the negatively charged flexible C-terminal ends of the fibrils. These intermolecular interactions reduce intramolecular contacts in monomeric α-Syn, yielding further unfolding of the partially collapsed intrinsically disordered states of α-Syn along with a possible increase in the local concentration of soluble α-Syn and alignment of individual monomers on the fibril surface. Our data indicate that intramolecular unfolding critically contributes to the aggregation kinetics of α-Syn during secondary nucleation.

α-synuclein | protein aggregation | secondary nucleation | Parkinson's disease

Synucleinopathies, including Parkinson's disease (PD), are associated with the accumulation of intracellular neuronal aggregates termed as Lewy bodies and Lewy neuritis, which contain high concentration of the protein α-synuclein (α-Syn) in an aggregated state (1, 2). The disease-relevant role of α-Syn is further highlighted by mutations in the α-Syn gene (SNCA) causing familial PD [i.e., A30P (3), E46K (4), H50Q (5), G51D (6), A53E (7), and A53T (8)] and the duplication or triplication of the SNCA leading to early-onset PD in affected families (9, 10). α-Syn is a 140-residue intrinsically disordered protein (IDP) in solution (11) but adopts a helical structure in the presence of acidic lipid surfaces (12, 13). The positively charged N terminus (residues 1 to 60) is rich in lysine residues and contains KTKEGV binding repeats associated with vesicle binding (14). Moreover, the N-terminal domain includes all known SNCA familial PD mutations. The central region (residues 61 to 95) defines the non-amyloid-β component (NAC) (15), which is essential for α-Syn aggregation (16), while the C terminus (residues 96 to 140) is highly negatively charged.

In vitro, α-Syn forms polymorphic amyloid fibrils (17–19) with unique arrangements of cross-β-sheet motifs (20–22). When injected into model animals, these fibrils induce a PD-like pathology (23) where the aggregation pathway of α-Syn plays a key role in the development of the disease (24). A detailed analysis of the aggregation kinetics of α-Syn into amyloids is therefore important toward understanding the toxic mechanisms relevant for synucleinopathies.

Amyloid formation of α-Syn is very sensitive to solution conditions, including pH (25), temperature (26), and salt concentration (27). It further requires the presence of an air–water interface (28) or negatively charged lipid membranes (29) for which α-Syn has a high affinity. Previous studies suggest that amyloid fibril growth of α-Syn occurs via a nucleation-dependent polymerization reaction (30). Following a fairly slow primary nucleus formation, α-Syn fibrils are elongated by addition of single monomers. In a next step, the amyloid fibrils multiply by fragmentation or can catalyze the formation of new amyloids from monomers on their surface—a process known as secondary nucleation that was first described for sickle cell anemia 40 y ago (31). Fragmentation and secondary nucleation critically depend on the fibril mass and accelerate the aggregation kinetics (30). In the case of α-Syn aggregation under quiescent condition fragmentation does not exist and only the described secondary nucleation process occurs. While detailed kinetic experiments showed no significant secondary nucleation at pH 7, it strongly contributes at pH values lower than 6 (25, 30). However, mechanistic or structural information of the secondary nucleation process in α-Syn aggregation has been lacking so far.

In this study we investigated the structural properties of α-Syn monomer–fibril interactions by NMR and electron paramagnetic resonance (EPR) spectroscopy. Our results provide insights into how monomeric α-Syn transiently interacts in vitro via its positively charged N terminus with the negatively charged C-terminal residues of the α-Syn fibrils, giving detailed insights into the mechanism of the secondary nucleation process.

Significance

The characteristic feature of Parkinson's disease is the deposition of α-synuclein into insoluble amyloid fibrils. The so-called secondary nucleation mechanism appears to be key for the aggregation kinetics, because binding of monomers on the fibril surface can autocatalytically induce new amyloid seeds. We show by nuclear magnetic and electron paramagnetic resonance spectroscopy that α-synuclein monomer–fibril binding is primarily mediated by transient electrostatic interactions. These intermolecular contacts result in an unfolding of the loosely packed α-synuclein structures and expose the otherwise protected aggregation-prone non-amyloid-β component of the protein. Our data demonstrate that intramolecular unfolding of α-synuclein is a prerequisite for protein aggregation that leads to rapid multiplication of α-synuclein amyloid fibrils via the secondary nucleation process.

Author contributions: G.J., R.R., and C.E. designed research; P.K., D.G., A.V., Y.F., T.W., and C.E. performed research; C.E. contributed new reagents/analytic tools; P.K., D.G., A.V., Y.F., T.W., and C.E. analyzed data; and R.R. and C.E. wrote the paper.

The authors declare no competing interest.

This article is a PNAS Direct Submission.

[1]P.K. and D.G. contributed equally to this work.

[2]To whom correspondence may be addressed. Email: roland.riek@phys.chem.ethz.ch or cedric.eichmann@phys.chem.ethz.ch.

This article contains supporting information online at https://www.pnas.org/lookup/suppl/doi:10.1073/pnas.2012171118/-/DCSupplemental.

Published March 1, 2021.

Results and Discussion

Recapitulating Secondary Nucleation of α-Syn Aggregation. Knowles, Linse, and coworkers have demonstrated previously by seeded aggregation kinetics that in the absence of salt secondary nucleation of α-Syn is present at pH 7.4 but contributes much more strongly (by approximately four orders of magnitude) to the production of new growing fibrils at pH values below 6 (25, 30). To recapitulate qualitatively whether secondary nucleation of α-Syn existed under our NMR conditions (no salt, 25 mM sodium phosphate, pH 7, and 250 μM α-Syn) we investigated α-Syn aggregation kinetics by Thioflavin T (ThT) fluorescence (*SI Appendix*, Fig. S1*A*). In contrast to the studies mentioned before (25, 30) we used mature α-Syn seed fibrils without sonication (*Materials and Methods*) to bypass the primary nucleation reaction and to strengthen relatively the secondary nucleation effect versus fibril elongation (25, 32). By omitting sonication of the seeded fibrils we not only mimicked the situation of the liquid-state NMR experiments that follow (Fig. 1) but also reduced the contribution of fibril elongation in the ThT kinetics by ∼10- to 100-fold (*SI Appendix*, Fig. S1*B*) because the seeds are 10 to 100 longer than in the case of sonication, which helped to determine the secondary nucleation process. We systematically increased the concentration of seed fibrils from 0 to 60%, which was the lowest concentration that could be used for the NMR experiments (discussed below). The aggregation kinetics was measured under conditions free of fragmentation. In order to investigate whether fibril fragmentation was absent in our ThT assay, we collected negative-stain electron microscopy (EM) data of an α-Syn sample (3% seeds) after 84 h of incubation at 37 °C. The EM micrographs showed long α-Syn fibrils (*SI Appendix*, Fig. S1*A*), which confirmed that our almost quiescent conditions did not induce fibril fragmentation. In line with earlier reports (25, 30), comparison of the kinetic traces revealed shorter lag times at higher seed concentrations and no aggregation of α-Syn up to 94 h without added seed fibrils (*SI Appendix*, Fig. S1*A*). Together with global fitting of the kinetic traces (33) for 0.5 to 3% seeds (*SI Appendix*, Fig. S2) and the positive curvature of the kinetics for 10% seeds, our data supported the contribution of a fibril surface-catalyzed secondary nucleation process to the aggregation mechanism of α-Syn. In the 60% seed experiment the lack of a lag phase and the positive curvature attributed to the fast kinetics did, however, not allow us to discriminate between seeded elongation and secondary nucleation (*SI Appendix*, Fig. S1*A*). In summary, without sonication of the seeds these experiments confirmed that the aggregation kinetics of α-Syn shows strong signs of surface-catalyzed secondary nucleation giving rise to fibril proliferation even at pH 7, in contrast to previous results from aggregation assays using sonicated seed fibrils (25, 30).

Transient Interactions between α-Syn Monomer and Fibrils. We hypothesized that secondary nucleation processes in α-Syn aggregation require transient monomer–fibril surface interactions. To obtain information on the binding modes of monomeric α-Syn to mature α-Syn fibrils two-dimensional (2D) liquid-state ^{15}N-^{1}H correlation NMR spectra of N-terminally acetylated ^{15}N-labeled α-Syn in the presence of unlabeled α-Syn fibrils (seed fibrils 540%) were recorded at pH 7 without added salts. Analyzing residue-resolved signal intensity ratios (I/I_0) of fibril-bound and unbound monomeric α-Syn, we found attenuated signal intensities for residues 1∼40 attributed to transient interactions of α-Syn with the fibrils. I/I_0 increased continuously from the N terminus, indicating that residues 1 to 12 having only three charged (Lys6, 10, and 12) and one aromatic residue (Phe4) constituted the primary interaction sites. In contrast, for residues ∼41 to 100 I/I_0 plateaued, suggesting that this region of α-Syn did not interact with the fibrils (Fig. 1*A*). We detected no contributions to fibril binding by α-Syn residues in the vicinity of the C terminus.

To strengthen these findings, we measured transverse ^{15}N amide relaxation parameters R_2 as a function of fibril concentration (seed fibrils 60, 240, and 540%) at pH 7, because R_2 is sensitive to chemical exchange dynamics expected to be present in transient interactions between α-Syn monomers and fibrils. Indeed, the ∼20 N-terminal residues of α-Syn showed higher R_2 rates compared to α-Syn free in solution (Fig. 1*B*). Again, the highest response was observed for residues 1 to 10. Under our

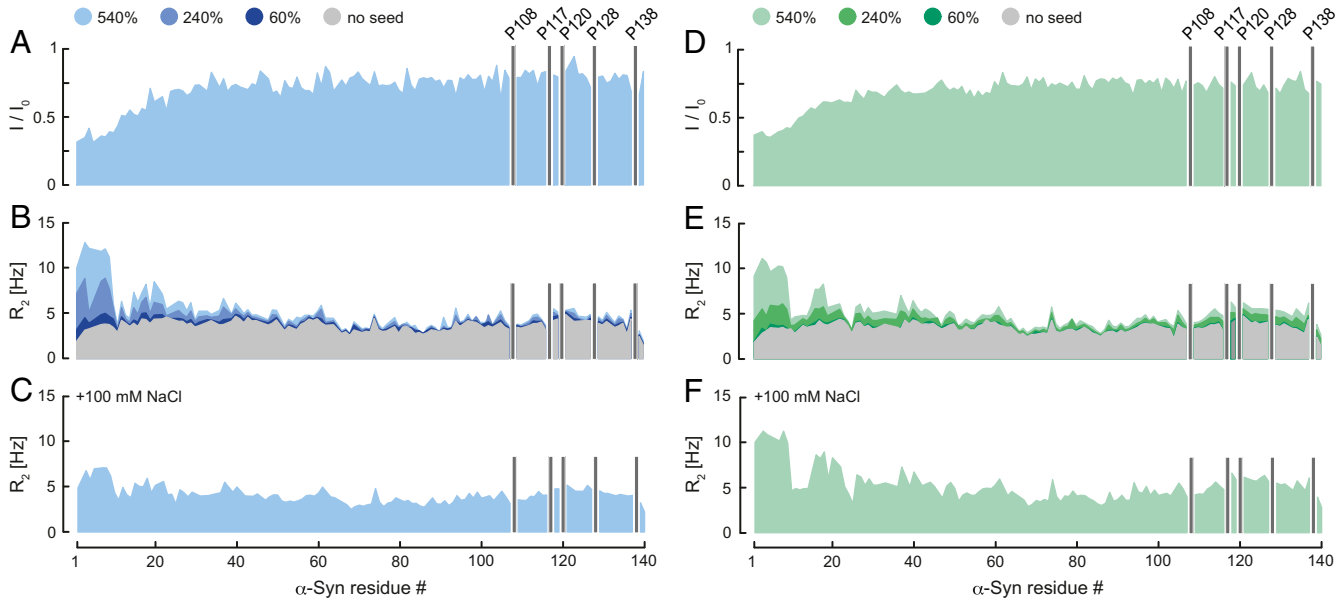

Fig. 1. Transient α-Syn monomer–fibril interaction. (*A* and *D*) Residue-resolved NMR signal intensity ratios (I/I_0) of fibril-bound (I) and unbound (I_0) α-Syn at pH 7 (blue) and 6 (green), no salt. ^{15}N R_2 relaxation rates of fibril-bound α-Syn in the (*B* and *E*) absence and (*C* and *F*) presence of 100 mM NaCl at pH 7 and 6. Seed concentrations are expressed as percentage of soluble α-Syn concentration. I/I_0 was determined at 540% α-Syn fibril seeds. R_2 rates were measured at 0, 60, 240, and 540% α-Syn fibril seeds. Positions of C-terminal α-Syn proline residues without peptide amide resonances are shown in one-letter amino acid code.

experimental conditions at pH 7 monomeric α-Syn aggregated slowly in the presence of fibrils during the 5-h measurement time (*SI Appendix*, Fig. S3). In addition, R_2 of the N-terminal region of α-Syn strongly increased with higher fibril concentration (Fig. 1*B* and *SI Appendix*, Fig. S4*A*), which allowed us to determine an equilibrium dissociation constant K_d and the number of binding sites on the α-Syn fibrils for the individual ^{15}N-^{1}H moieties of monomeric α-Syn. Using the Hill equation for n-binding sites yielded an average $K_d \approx 1$ mM and $n \approx 2$ (*SI Appendix*, Fig. S4*A*), indicating that on average each α-Syn molecule within the fibril had approximately two binding sites. For residues 21 to 140 we did not detect major differences for R_2 of α-Syn in the presence or absence of fibrils (Fig. 1*B*), corroborating that fibril interactions were established via the N terminus of monomeric α-Syn. To further investigate whether this transient monomer–fibril binding was mediated via charge–charge interactions, we measured R_2 rates of monomeric α-Syn in presence of α-Syn fibrils and 100 mM NaCl at pH 7. We reasoned that NaCl will interfere with electrostatic protein interactions between the positively charged N terminus of monomeric α-Syn and the negatively charged C terminus of α-Syn fibrils. In turn, we expected to observe a decrease of α-Syn R_2 rates compared to the corresponding data in the absence of NaCl (Fig. 1*B*). Indeed, we detected for residues 1 to 20 smaller R_2 rates (Fig. 1*C*), indicating that α-Syn monomer–fibril interactions include a charge–charge nature.

Following these results we asked whether α-Syn monomer–fibril interactions were pH-dependent. To answer this question, we recorded liquid-state NMR data at pH 6. Similar to pH 7, the I/I_0 and R_2 profile of α-Syn in presence of fibrils without added salt showed that residues 1∼20 constituted the main interaction sites of monomeric α-Syn with the fibrils (Fig. 1 *D* and *E*). In contrast to pH 7, ∼50% of monomeric α-Syn aggregated upon addition of fibrils at pH 6 (5-h measurement time), thus making it not possible to determine a K_d by using the Hill equation (*SI Appendix*, Figs. S3 and S4*B*). However, at pH 6 the presence of 100 mM NaCl did not substantially reduce the R_2 rates (Fig. 1*F*), suggesting a higher binding affinity of α-Syn monomers to fibrils at physiological salt conditions and pH 6 when compared to pH 7 (34) (Fig. 1*C*), in line with the reported pH dependence of secondary nucleation (25). Mildly acidic pH conditions are found, for example, in endosomes, and thus our in vitro results at pH 6 in presence of 100 mM NaCl mimic conditions found in cellular environments. From these experiments we concluded that electrostatic monomer–fibril interactions alone did not suffice for α-Syn binding and suspected that pi–pi interactions between aromatic side chains contribute to the secondary nucleation process.

Knowing that the oppositely charged N- and C-terminal segments of monomeric α-Syn and fibrils interact, we then performed NMR experiments with mutant forms of α-Syn in which we deleted residues 2 to 11 (ΔN), substituted the positively charged Lys6, Lys10, and Lys12 with alanine (K6A;K10A;K12A), or removed the negative charges from the C terminus of the fibrils truncating α-Syn at position Asp121 (ΔC). In line with our results at pH 7, we neither observed an increase of R_2 for α-Syn(ΔN) and α-Syn(K6A;K10A;K12A) in presence of α-Syn fibrils nor for α-Syn upon addition of α-Syn(ΔC) fibrils (Fig. 2 *A*–*C*), verifying that α-Syn monomer–fibril interactions depended on intact charged N and C termini of α-Syn. These findings were supported by additional ThT kinetic experiments using nonsonicated α-Syn(ΔC) fibrils. As observed previously for soluble α-Syn, the kinetic traces of α-Syn in presence of α-Syn(ΔC) seeds showed no signs of aggregation up to ∼82 h (*SI Appendix*, Fig. S1*C*). Only full-length α-Syn seed fibrils were able to trigger aggregation of α-Syn, thus confirming the importance of electrostatics in transient monomer–fibril interactions that lead to fibril growth by surface-catalyzed secondary nucleation (*SI Appendix*, Fig. S1*A*).

To determine whether pi–pi interactions between the N and C termini of monomeric α-Syn and fibrils play a role in secondary nucleation, we mutated Phe4 and Tyr39 into alanine (F4A;Y39A) and measured R_2 rates of α-Syn(F4A;Y39A) in the presence of α-Syn fibrils at pH 6. Similar to our fibril binding results of wild-type α-Syn (Fig. 1*E*), we detected increased R_2 values for Ala4-Ser9, indicating α-Syn(F4A;Y39A) fibril interactions (Fig. 2*D*). It further suggests that in absence of salt the electrostatics dominated over the aromatic contributions in α-Syn fibril binding. We then prepared the same sample at pH 6 but added 100 mM NaCl. Because charge–charge α-Syn–fibril interactions were greatly reduced in the presence of salt, we expected that pi–pi contacts

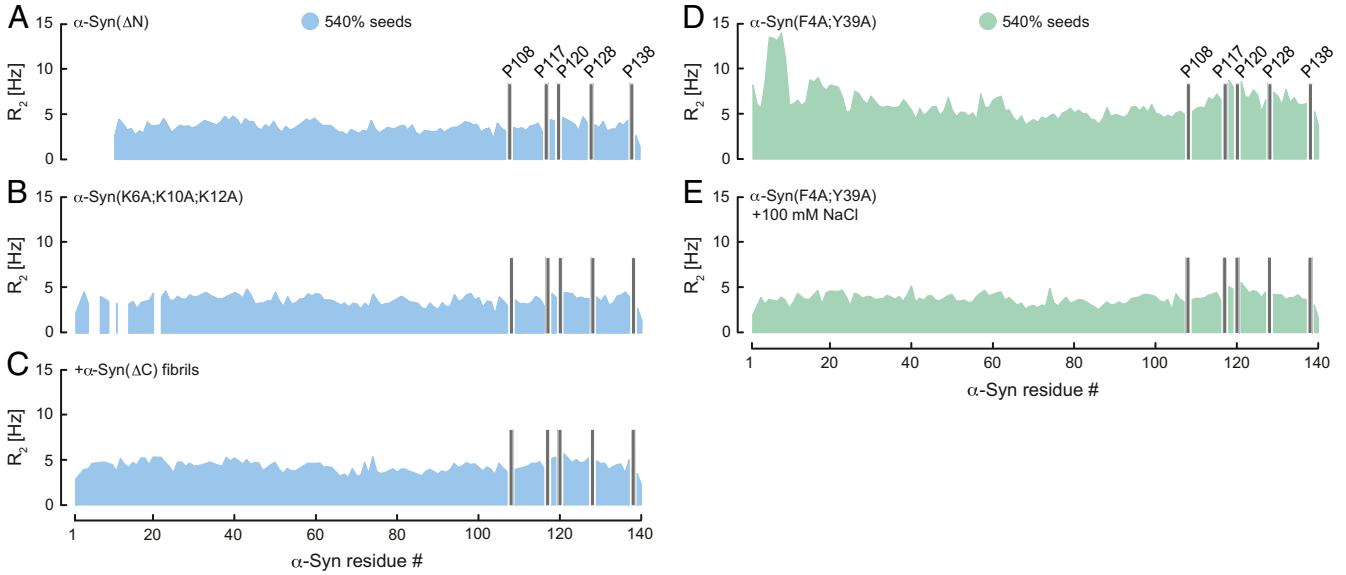

Fig. 2. Transient α-Syn mutant monomer–fibril interaction. Residue-resolved ^{15}N R_2 relaxation rates of (*A*) α-Syn(ΔN), (*B*) α-Syn(K6A;K10A;K12A), and (*C*) α-Syn in presence of wild-type α-Syn and α-Syn(ΔC) fibrils at pH 7. R_2 of α-Syn(F4A;Y39A) upon addition of wild-type α-Syn fibril seeds in the (*D*) absence and (*E*) presence of 100 mM NaCl at pH 6. Seed concentration is expressed as percentage of soluble α-Syn concentration. Positions of C-terminal α-Syn proline residues without peptide amide resonances are shown in one-letter amino acid code.

through Phe4 and Tyr39 become important for fibril binding under this condition. We measured again R_2 rates of α-Syn(F4A;Y39A), which revealed a uniform profile indicating that α-Syn(F4A;Y39A) at pH 6 in the presence of salt did not interact with α-Syn fibrils (Fig. 2*E*). Thus, these findings provide evidence that in addition to electrostatics aromatic pi–pi interactions critically contribute to transient α-Syn fibril-binding events.

Loosely Packed α-Syn Unfolds Further upon Binding to α-Syn Fibrils. To investigate the conformations of fibril-bound α-Syn, we performed NMR nuclear Overhauser enhancement (NOE), paramagnetic relaxation enhancement (PRE), and EPR double electron–electron resonance (DEER) measurements. Although α-Syn is classified as an IDP, previous PRE and DEER experiments on isolated (35) and cellular α-Syn (11) showed transient long-range intramolecular interactions between N- and C-terminal residues. These intramolecular contacts result in partially collapsed IDP states of α-Syn that deviate from extended polypeptide chain conformations and protect the central NAC region of the protein from aggregation (35). Cryo-EM data demonstrated that the C-terminal residues are not involved in the fibrillar core structure of all known α-Syn polymorphs (36) and C-terminal truncated α-Syn constructs are more prone to aggregation (20, 37).

Having established that monomeric α-Syn transiently interacted with its fibrils via the N-terminal segment, we asked the questions whether these intermolecular interactions will 1) induce the formation of structured α-Syn species on the fibril surface and 2) weaken the intramolecular contacts between the N and C termini in fibril-bound α-Syn, yielding a more unfolded α-Syn conformation. To determine short-range interactions (≤5 Å) in transiently fibril-bound α-Syn we analyzed three-dimensional (3D) ^{15}N-resolved [^{1}H,^{1}H]-NOESY (NOE spectroscopy) spectra of 150 μM ^{15}N-labeled α-Syn in presence of 1 mM unlabeled α-Syn fibrils (*SI Appendix*, Fig. S5*A*). Isolated α-Syn in solution adopts a so-called random coil structure, meaning that the protein comprises a rapidly interconverting mixture of many different conformers. They cover the possible structural space of the peptide sequence yielding NOEs between proton spin pairs. From a biophysical point of view, the NOE is thereby an ensemble-average measure. Because the α-Syn fibril concentration of 1 mM corresponds to the K_d of the monomer–fibril interaction, under our experimental conditions of the NOESY experiment in the presence of fibrils 50% of ^{15}N-labeled α-Syn is transiently bound to the fibrils, that is, in fast exchange with the fibrils. In line with these calculations, a comparison of the NOESY spectra of α-Syn with and without fibrils revealed that transverse relaxation of the α-Syn magnetization during the INEPT (insensitive nuclei enhancement by polarization transfer) resulted in a reduction of the $^1H^N$-$^1H^N$ diagonal peak intensities by ∼50% specific for the 10 N-terminal residues that are in fast exchange with the fibrils (*SI Appendix*, Fig. S5*B*). During the NOESY mixing there is no transverse relaxation and the NOE information is stored entirely. Apart from short-range NOEs typically observed for IDPs we did not detect any additional NOEs, either long-range, medium-range, or sequential-range NOE contacts, in transiently fibril-bound α-Syn (*SI Appendix*, Fig. S5*A*), which suggests that both transiently fibril-bound and isolated α-Syn were on average in a random-coil conformation. NMR spectroscopy is thereby not sensitive enough to exclude that a small percentage of α-Syn molecules might undergo a conformational change when bound to the fibril surface.

We then used PRE from site-directed spin labeling for the detection of long-range intramolecular contacts (∼15 Å) in fibril-bound α-Syn. Because the primary sequence of α-Syn does not include cysteine residues for paramagnetic MTSL labeling we created the α-Syn mutant A90C (*SI Appendix*, Fig. S6), which showed an NMR fingerprint spectrum very similar to wild-type α-Syn with negligible chemical shift changes except for residues around Cys90 (*SI Appendix*, Fig. S6), indicating that α-Syn(A90C) behaves structurally and dynamically as the wild-type protein. MTSL-labeled α-Syn(A90C) caused quenching of nearby ^{15}N-^{1}H moieties in a 2D ^{15}N-^{1}H correlation NMR spectrum. The cross-peak intensity ratios between two ^{15}N-^{1}H correlation NMR spectra in the presence and absence of the paramagnetic MTSL-tag (I_{param}/I_{diam} in Fig. 3*A*) revealed for α-Syn(A90C) a broad paramagnetic line broadening for Val40 to Asp135, suggesting partial collapsed IDP states of soluble α-Syn, as previously documented (35). Addition of α-Syn fibrils reduced the paramagnetic quenching effect in the C-terminal region and, interestingly, for residues located in the preNAC and NACore (38) (Fig. 3*A*), indicating an unfolding of the partially collapsed conformations of α-Syn by destabilizing the electrostatic interactions between the N and C terminus when the protein interacted with fibrils. This finding is in agreement with a previous PRE study using the α-Syn(A90C) mutant: Similar to the urea-denaturated state of the protein, binding of polycations to the C-terminal residues led to a minimization of paramagnetic broadening in the C terminus,

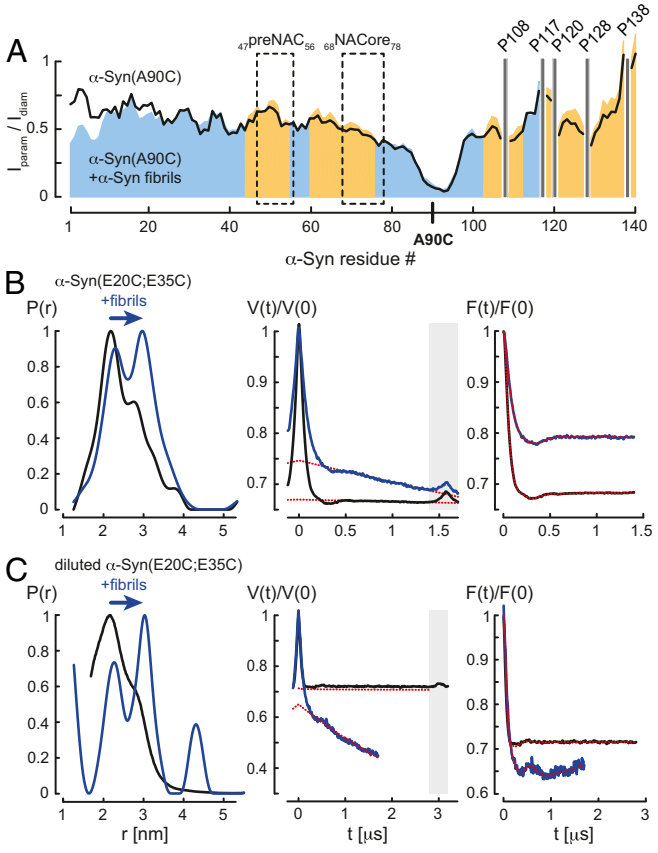

Fig. 3. Unfolding of fibril-bound α-Syn. (*A*) Residue-resolved PRE intensity profiles I_{param}/I_{diam} of para- (I_{param}) and diamagnetic (I_{diam}) labeled α-Syn(A90C) in the absence (black) and presence of 5.4-fold molar excess of α-Syn fibrils (blue) at pH 7. Regions with increased I_{param}/I_{diam} values in presence of α-Syn fibrils compared to soluble α-Syn(A90C) are colored in orange. The preNAC and NACore regions of α-Syn are highlighted. Positions of C-terminal α-Syn proline residues without peptide amide resonances are shown in one-letter amino acid code. (*B*) EPR measurements of MTSL-labeled α-Syn(E20C;E35C) and (*C*) partially MTSL-labeled α-Syn(E20C;E35C) in the absence (black) and presence (blue) of α-Syn fibrils, monomer:fibril molar ratio 1:10, at pH 7. From left to right, distance distributions P(r) using DeerAnalysis2019, primary Q-band DEER data V(t)/V(0), and background-corrected form factors F(t)/F(0) are shown including homogeneous background fits (red dotted lines). Time traces within the gray boxes were excluded from the background.

pointing to an electrostatic interaction between the oppositely charged N and C termini of α-Syn (35).

In order to investigate the mechanism of intramolecular α-Syn unfolding in more detail, we produced the MTSL-labeled α-Syn(ΔN;A90C) and α-Syn(K6A;K10A;K12A;A90C) mutants (*SI Appendix*, Fig. S6) and performed PRE experiments on the monomeric proteins. They revealed that N-terminal truncation or removal of the positive charges at the N terminus of α-Syn restricted paramagnetic broadening within the NACore (*SI Appendix*, Fig. S7 *A–C*), indicating that α-Syn was further unfolded in absence of intramolecular electrostatic contacts between the N and C terminus. Moreover, ThT kinetics showed that α-Syn(K6A;K10A;K12A), being more unfolded and comprising a less-protected NACore, aggregated faster than wild-type α-Syn (*SI Appendix*, Fig. S1*D*). However, in presence of wild-type α-Syn fibrils we observed for both proteins the same aggregation behavior with a reduced lag phase (*SI Appendix*, Fig. S1*D*). Our results suggest that fibril binding yielded a further unfolding only for wild-type α-Syn but not for α-Syn(K6A;K10A;K12A) because the mutant already adopted an extended conformation. This leads to practically identical seeded aggregation kinetics for wild-type and mutant α-Syn.

To further corroborate our PRE result we produced the α-Syn(E20C;E35C) mutant and performed intramolecular DEER experiments to determine the distances between the two MTSL-labeled cysteines. Chemical shift differences of ^{15}N-^{1}H resonances between wild-type α-Syn and α-Syn(E20C;E35C) were only detected at the mutation sites, indicating that both proteins adopt intrinsically disordered conformations with similar dynamics (*SI Appendix*, Fig. S6). In the absence of fibrils, monomeric MTSL-labeled α-Syn(E20C;E35C) yielded a broad distance distribution attributed to the intrinsically disordered character of the protein covering different conformational states with a main population at ∼2.2 nm and a minor shoulder at slightly larger distances (Fig. 3*B*). However, addition of α-Syn fibrils to this sample (monomer:fibril molar ratio 1:10) resulted in two distinctive separate distance populations at ∼2.3 and 3 nm (Fig. 3*B*). The short distance was indicative of the soluble α-Syn structures, also observed in the sample without fibrils. The increase of the population corresponding to the larger distance suggested that α-Syn–fibril interactions weakened the intramolecular contacts, favoring more extended conformations of the protein. To validate our conclusion that the larger distance originated from fibril-bound α-Syn and did not result from intermolecular interactions between monomers as they assemble on the surface of the fibril, we performed DEER experiments with partially MTSL-labeled α-Syn(E20C;E35C) (1:2 effective spin dilution). As observed for 100% MTSL-labeled α-Syn(E20C;E35C), spin dilution of the monomeric protein yielded a main population at ∼2.2 nm and a minor shoulder at slightly longer distances, whereas the presence α-Syn fibrils (monomer:fibril molar ratio 1:10) revealed again two well-defined distances at ∼2.3 and 3 nm (Fig. 3*C*; note that the peak at ∼4.2 nm is an artifact due to incomplete background correction). Together, these findings suggested that indeed the presence of the larger distance in fibril-bound α-Syn(E20C;E35C) was of an intramolecular nature, thus providing evidence that binding of α-Syn to fibrils results in unfolding of the protein.

Negatively Charged C Termini of the α-Syn Fibrils Lower the Local pH on the Fibril Surface. Previous work has shown large differences between random-coil and α-Syn pK_a (negative logarithm of association constant) values. Lowered respectively raised pK_a values were observed in the N and C terminus of monomeric α-Syn (39), thereby providing additional evidence for the presence of weak long-range intramolecular electrostatic interactions between the N- and C-terminal residues. Because the fuzzy coat of the acidic C-terminal segment of the α-Syn fibril can be interpreted as a negatively charged surface with a high concentration of glutamic acids, we expected that fibril-localized H_3O^+ decreases the pH on the surface of the α-Syn fibrils approximately by one pH unit. When measuring the pH in the bulk yields an increase of the pK_a values of the Glu residues in the C terminus of the fibrils by about one unit compared to monomeric α-Syn. To determine this fibril-induced pH change, we recorded magic-angle spinning (MAS) solid-state ^{13}C NMR spectra of ^{13}C, ^{15}N-labeled α-Syn fibrils at pH 7 and 6. Selective excitation of the mobile regions of the α-Syn fibrils through an INEPT proton-to-carbon transfer revealed narrow lines with the typical resonance set for Glu (Fig. 4*A* and *SI Appendix*, Fig. S8). We used the Glu $^{13}C^{\gamma}$ carbon chemical shift as a pH probe because of its large change on the order of 4 ppm from neutral to acidic pH (39). The one-dimensional (1D) ^{13}C MAS INEPT NMR spectrum showed chemical shifts of 36.2 (pH 7) and 35.8 ppm (pH 6) for Glu C^{γ} (Fig. 4*A*), which were ∼0.7 and 0.9 parts per million (ppm) smaller than the corresponding values in monomeric α-Syn (Fig. 4*B*) (39). Comparing the Glu $^{13}C^{\gamma}$ chemical shifts of the fibrils with the pH titration data of Glu114 in monomeric α-Syn (39) indicated that the local pH values on the surface of the α-Syn fibrils were significantly lower (pH ∼5.4 and 5.1) than in the bulk (pH 7 and 6; Fig. 4*B*). This in turn suggests that compared to the bulk the Glu side-chain pK_a values within the C terminus of α-Syn fibrils are indeed higher than in monomeric α-Syn.

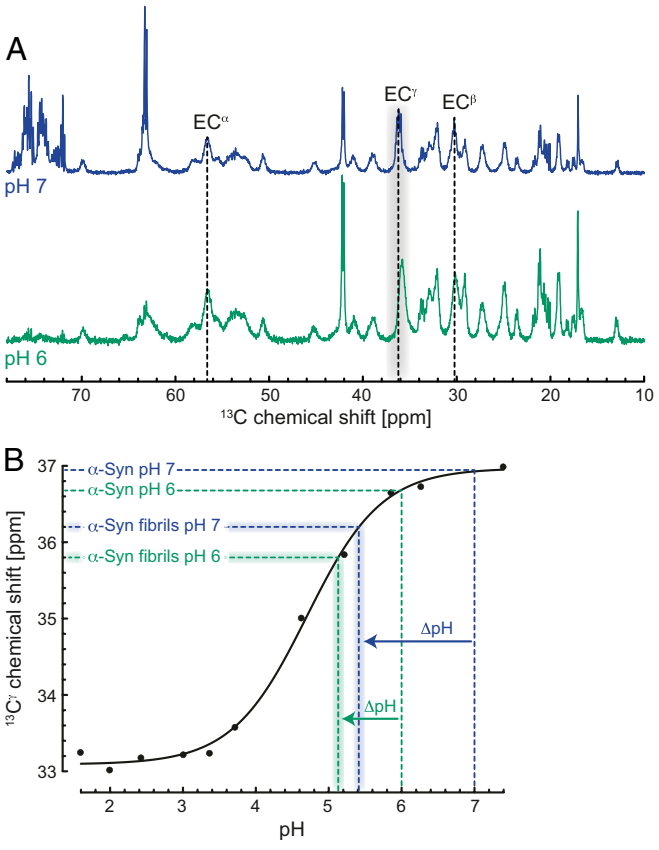

Fig. 4. Lowered local pH on the surface of the α-Syn fibrils triggers monomer–fibril interactions. (*A*) One-dimensional (1D) ^{13}C MAS INEPT NMR spectra of the mobile regions of α-Syn fibrils at pH 7 (blue) and 6 (green) in the absence of salt. ^{13}C chemical shifts of Glu residues are shown in one-letter amino acid code. (*B*) Comparison of the pH titration data reported for Glu114 $^{13}C^{\gamma}$ of soluble α-Syn (black, reproduced from ref. 39) and the Glu $^{13}C^{\gamma}$ chemical shifts of the α-Syn fibrils obtained from the 1D ^{13}C INEPT spectrum. The local ΔpH differences between soluble and α-Syn fibrils at pH 7 (blue) and 6 (green) are indicated.

Mechanistic Insights into the Secondary Nucleation Process of α-Syn. Our NMR data provide evidence that weak transient α-Syn monomer–fibril interactions in the millimolar range are present both at pH 7 and 6 (Fig. 1). α-Syn binds with its positively charged N-terminal segment to the negatively charged flexible C-terminal tails of the fibrils with approximately two binding sites per α-Syn molecule in the fibril. Only at pH 6 these interactions did not depend much on the salt concentration, indicating that in addition to charge–charge attraction (Fig. 2 *A*–*C*), pi–pi interactions via the aromatic residues contribute to the observed α-Syn monomer–fibril binding events (Fig. 2 *D* and *E*). The intermolecular interactions thereby compete with transient long-range intramolecular contacts between N- and C-terminal residues in monomeric α-Syn, yielding an unfolding of the partially collapsed intrinsically disordered states of monomeric α-Syn (Fig. 5). We believe that this process can dynamically align α-Syn molecules at high local concentrations on the surface of amyloid fibrils, which exposes the otherwise protected NAC region of the protein (Fig. 5). This results in a powerful de novo aggregation mechanism described previously by kinetic studies as secondary nucleation (31). In this scenario N-terminally modified (*SI Appendix*, Fig. S1*D*) or C-terminally truncated α-Syn do not follow the proposed secondary nucleation mechanism because the protein is already fully unfolded with an exposed NAC region (37). Our findings are additionally supported by recent data showing that the α-Syn seeding process is initiated by monomer recruitment on the fibril surface through the intrinsically disordered N and C termini (40).

In line with our study, it was demonstrated that secondary nucleation of α-Syn below pH 6 very weakly depends on the ionic strength of the buffer (30) but is strongly reduced in absence of the C-terminal region of the protein (41). At pH 5 the intra- and intermolecular charge–charge interactions within α-Syn monomers and between monomers and fibrils start to disappear (the pK_a of Glu is ∼4.3). Because monomeric α-Syn interacts with a large array of C-terminal fibril ends residual intermolecular charge–charge interactions between α-Syn and fibrils remain present (Fig. 5). In other words, from bulk pH 6 to pH 5 the intramolecular contacts are weakened more than the intermolecular interactions. This is attributed to the higher pK_a values of the negatively charged C-terminal Glu residues of the α-Syn fibrils when compared with corresponding monomeric entities (Fig. 4*B*).

In this context it is interesting to note that unfolding of locally concentrated and aligned α-Syn molecules as a prerequisite for α-Syn aggregation by the secondary nucleation mechanism (Fig. 5) may also happen at the air–water interphase (28) or on negatively charged membranes (29). α-Syn does not aggregate de novo in absence of an air–water interphase while fibrils only elongate (28), and α-Syn aggregation is enhanced by the presence of negatively charged membranes (29) (in the absence of salt and as long as the membrane concentration is low). The attraction of α-Syn monomers to the air–water interphase and to negatively charged membranes may thus also yield a high local concentration of aligned and entirely unfolded α-Syn monomers, which form a nucleus for aggregation.

In conclusion, we present mechanistic insights into the secondary nucleation process of α-Syn associated with PD. The in vitro data highlight that transient α-Syn monomer–fibril binding unfolds the partially collapsed intrinsically disordered states of the protein. At α-Syn fibril concentration of K_d ∼1 mM, 50% of monomeric α-Syn is in a transient fibril-bound state. Because we observe an interaction of the N terminus of α-Syn with the C termini of the structurally ordered fibrils some degree of molecular alignment of fibril-bound α-Syn is requested. In addition, the weak binding of the α-Syn monomers along with the possible restricted 2D diffusion on the surface of the fibrils locally concentrates α-Syn monomers. Thereby, the α-Syn fibrils generate an environment that supports de novo nucleus formation termed

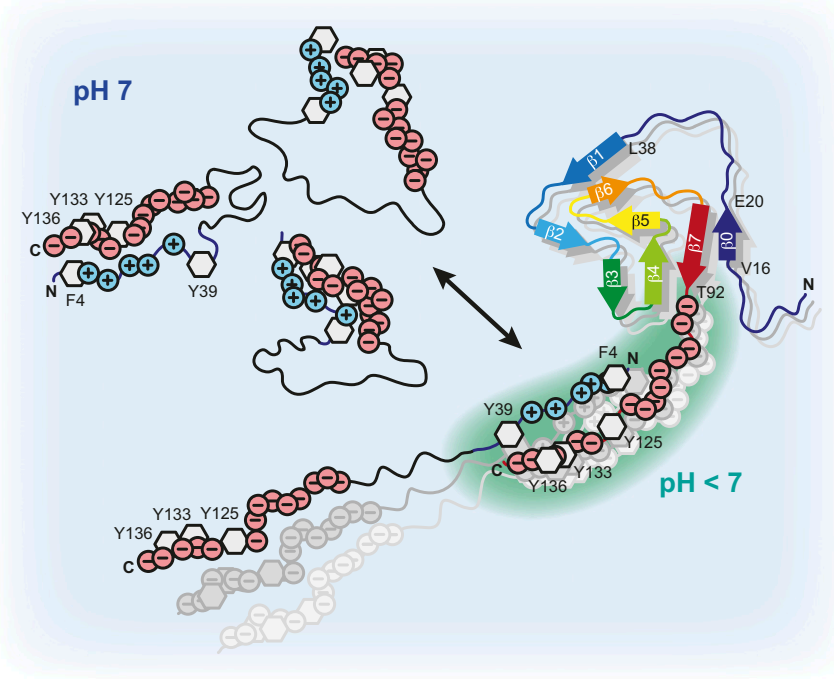

Fig. 5. Scheme of α-Syn fibril interactions. Transient long-range intramolecular contacts between N- and C-terminal residues in soluble α-Syn yield partially collapsed intrinsically disordered states of the protein and occlude the central aggregation-prone NAC region. The highly negatively charged C terminus of the α-Syn fibrils lowers the local pH compared to the bulk. Intermolecular α-Syn-fibril interactions between the positively charged N-terminal segment of α-Syn and the negatively charged flexible C-terminal tails of the fibrils unfold the loosely packed α-Syn structures and dynamically align α-Syn molecules at high local concentrations on the fibril surface. This results in an exposure of the NAC region and triggers protein aggregation via secondary nucleation.

secondary nucleation, which results in a multiplication of amyloid fibrils reminiscent of an autocatalytic process with disease-devastating potential. Spreading of these α-Syn aggregates in the brain between neighboring cells occurs in a prion-like manner (42) and can be described by the presence of a secondary nucleation mechanism that strongly depends on solution conditions and rapidly increases below pH 6 (25). Accelerated prion-like protein aggregation is found, for example, in the mildly acidic chemical environment of endosomes (43). Thus, our findings not only provide insights into the aggregation mechanisms of α-Syn but also allow us to localize cellular compartments where pathological aggregation of α-Syn in PD may happen.

Materials and Methods

Recombinant Protein Expression and Purification. N-terminally acetylated, human wild-type α-Syn was produced by coexpressing the pRK172 plasmid with the yeast N-acetyltransferase complex B (NatB) (44) in *E. coli* BL21 Star (DE3) cells using Luria–Bertani broth (unlabeled α-Syn) and M9 minimal media supplemented with $^{13}C_6$-D-glucose and $^{15}NH_4Cl$ (^{13}C and ^{15}N, ^{15}N-labeled α-Syn). Protein purification was performed as described (28). α-Syn mutants ΔN, (K6A;K10A;K12A), ΔC, (F4A;Y39A), A90C, (ΔN;A90C), (K6A;K10A;K12A;A90C), and (E20C;E35C) were generated by site-directed mutagenesis (QuikChange; Agilent Technologies) and confirmed by DNA sequencing. With the exception of α-Syn(ΔN) and α-Syn(ΔN;A90C), recombinant protein expression and purification of α-Syn mutants were identical to wild-type α-Syn. Five millimolar β-mercaptoethanol was added to the α-Syn Cys mutant samples to keep the cysteines in their reduced state. Lacking the N-terminal substrate specificity for NatB, α-Syn(ΔN) and α-Syn(ΔN;A90C) were produced in their nonacetylated forms. Protein concentrations were determined spectrophotometrically by ultraviolet absorbance measurements at 280 nm. For α-Syn(F4A;Y39A) and α-Syn(ΔC), ε = 4,470 and 1,490 $M^{-1}{\cdot}cm^{-1}$ were used. For all other α-Syn constructs ε = 5,960 $M^{-1}{\cdot}cm^{-1}$ was used. Protein samples were concentrated to 1 mM in NMR buffer (25 mM sodium phosphate) at pH 7 or 6. Final aliquots of protein stock solutions were snap-frozen in liquid nitrogen and stored at −80 °C until use. To remove oligomeric species from monomeric protein, all samples were filtered with a 100-kDa molecular weight cutoff concentrator (Amicon) before NMR and EPR sample preparation.

Amyloid Fibril Preparation. For the formation of mature fibrils, Eppendorf tubes (1.5 mL) containing 0.5 mL of 500 μM α-Syn and α-Syn(ΔC) in NMR buffer at pH 7 or 6, 150 mM NaCl, and 0.02% NaN_3 were incubated at 37 °C on a rotating mixer at 30 rpm for 2 to 3 wk. To remove the salt before NMR measurements, fibrils were pelleted by centrifugation and washed with NMR buffer at pH 7 or 6 (three times).

Spin Labeling of α-Syn Cysteine Mutants. Spin labeling of the α-Syn Cys mutants with paramagnetic MTSL and its diamagnetic analog (Toronto Research Chemicals) was performed in NMR buffer at pH 7 as described previously (45). To remove higher molecular α-Syn species after MTSL-labeling, the proteins were filtered using a 100-kDa molecular weight cutoff concentrator (Amicon). MTSL-labeling efficiency was determined by continuous-wave EPR at protein concentrations of 100 μM in a 0.9-mm-outside-diameter (OD) glass capillary.

ThT Fluorescence Assay. Aggregation and amyloid formation of wild-type α-Syn and α-Syn mutants at protein concentrations of 300 μM in NMR buffer at pH 7, 0.02% sodium azide, total sample volume 0.5 mL, was initiated in the presence and absence of different concentrations of preformed seed fibrils in 1.5-mL Eppendorf tubes. Seeding experiments were performed with nonsonicated mature wild-type α-Syn fibrils at 0.5, 1, 3, 10, and 60% and α-Syn(ΔC) fibrils at 3% of the concentration of monomeric protein with gentle agitation at 30 rpm, 37 °C. These conditions are considered to be quiescent because negative-stain EM of these samples showed in general micrometer-long α-Syn fibrils (*SI Appendix*, Fig. S1*A*). In a control experiment, preformed fibrils were sonicated on ice for 7, 15, and 35 min using a probe sonicator, 25% amplitude with constant pulse on and off times of 1 and 3 s. For ThT fluorescence measurements, 4 μL of the samples were diluted with 200 μL of NMR buffer at pH 7, 0.02% sodium azide, and 2 μL of 1 mM freshly prepared ThT solution (20 mM Tris·HCl, pH 8.0) was added. ThT fluorescence data were recorded on a Horiba-Jobin Yvon (FluoroMax 4) spectrofluorometer operating at an excitation wavelength of 450 nm and emission in the range of 465 to 500 nm with a slit width of 5 nm (both for excitation and emission). Processing and analysis of the wild-type α-Syn aggregation kinetics were performed with AmyloFit (33).

Liquid-State NMR Sample Preparation. NMR samples were prepared in NMR buffer at pH 7 or 6. ^{15}N-labeled protein concentrations for 2D liquid-state NMR were adjusted to 250 μM. NMR signal intensity ratios (I/I_0) were determined in the presence (I) and absence (I_0) of 1.35 mM (5.4-fold molar excess) unlabeled wild-type α-Syn fibrils. ^{15}N transverse R_2 titration of α-Syn was collected at pH 7 and 6 in the absence of fibrils and upon addition of 0.6-, 1.2-, 1.8-, 2.4-, 3.6-, 4.2- (only pH 7), 4.8-, 5.4-, and 7.2-fold (only pH 7) molar excess of unlabeled α-Syn fibrils. R_2 rates of α-Syn mutants were determined in the presence of 5.4-fold molar excess of unlabeled α-Syn fibrils. In addition, R_2 of α-Syn was determined upon addition of 5.4-fold molar excess of unlabeled α-Syn(ΔC) fibrils. I_{param}/I_{diam} intensity ratios of para- and diamagnetic labeled α-Syn mutants were collected on isolated protein samples and in the presence of 5.4-fold molar excess of unlabeled α-Syn fibrils. NOESY experiments were recorded on 150 μM ^{15}N-labeled α-Syn in the absence and presence of 6.7-fold molar excess of unlabeled α-Syn fibrils. Without incubation, all NMR samples were immediately measured after adding ^{15}N-labeled monomeric protein to the fibrils.

EPR Sample Preparation. Low-temperature EPR measurements were recorded on 25 μM MTSL-labeled α-Syn(E20C;E35C) free in solution and upon addition of 250 μM α-Syn fibrils. Control experiments were recorded on MTSL-labeled α-Syn(E20C;E35C) mixed with unlabeled α-Syn(E20C;E35C) at 1:2 effective spin dilution, 25 μM total protein, in the absence and presence of 250 μM α-Syn fibrils. EPR samples were mixed with 30% (vol/vol) glycerol as a cryoprotectant (sample volume 40 μL), transferred into 3-mm-OD annealed quartz capillaries (New Era Enterprises), flash-frozen in precooled isopentane, and stored at −80 °C until use.

Liquid-State NMR Spectroscopy. All NMR samples were supplemented with 4% D_2O, total volume 320 μL, and transferred into 5-mm (diameter) Shigemi tubes. NMR experiments were performed on a Bruker 600 MHz Avance III HD spectrometer equipped with a cryogenically cooled proton-optimized $^1H\{^{13}C/^{15}N\}$ TCI probe. Reference and α-Syn-fibril NMR spectra were acquired with identical spectrometer settings and general acquisition parameters at 283 K. Specifically, we employed 2D ^{15}N-^1H SOFAST HMQC NMR pulse sequences (46) with a data size of 128 × 512 complex points for a sweep width (SW) of 28.0 ppm (^{15}N) and 16.7 ppm (^1H), 64 scans, 60-ms recycling delay (acquisition time ∼20 min). NMR signal intensity ratios (I/I_0) and (I_{param}/I_{diam}) were determined for each residue by extracting the maximal signal height of the cross-peaks from the respective 2D ^{15}N-^1H NMR spectra. ^{15}N transverse R_2 relaxation rates were measured using a Hahn-echo-based 2D ^{15}N-^1H NMR experiment as described previously (47), data size 80 × 512 complex points, SW of 27.6 (^{15}N) and 16.4 ppm (^1H). The magnetization decay was recorded at four different relaxation decay periods (0, 50, 100, and 200 ms) in an interleaved manner with 16 scans, acquisition time ∼5 h. The 3D ^{15}N-resolved [^1H,^1H]-NOESY experiments (48) were acquired with a NOE mixing time τ_m = 200 ms, 256 × 55 × 1,024 complex points, SW of 13.0 ppm (^1H), 35.2 ppm (^{15}N) and 14.3 ppm (^1H), and eight scans (acquisition time ∼2 d). All NMR spectra were processed with PROSA. Visualization and data analysis were carried out in CARA.

Solid-State NMR Spectroscopy. ^{13}C, ^{15}N-labeled α-Syn fibrils were packed into a 3.2-mm Bruker rotor by ultracentrifugation. Solid-state NMR experiments were performed on a Bruker 850-MHz wide-bore spectrometer equipped with a home-built 3.2-mm CONFINE-MAS probe (49) operating at MAS spinning frequency of 17.0 kHz. All NMR spectra were recorded at 283 K and referenced to 4,4-dimethyl-4-silapentane-1-sulfonic acid using the methylene resonance of solid adamantane as an external standard (50). INEPT experiments were recorded with an INEPT delay (1/4*J*) of 1.14 ms [$J(^1H$-$^{13}C)$ = 220 Hz], a repetition time of 1.5 s and 5-kHz WALTZ-64 proton decoupling during data acquisition; 1,024 and 2,048 scans were acquired for the pH 7 and 6 sample, respectively. The 2D INEPT spectrum was acquired with 16 scans and 2,048 increments in the indirect dimension (total acquisition time 15.4 ms). The 2D INEPT total through bond correlation spectroscopy experiment was recorded with the $C9_6^1$ scheme (mixing time 7.8 ms), 16 scans, and 512 increments in the indirect dimension (acquisition time 5.1 ms). The repetition time was set to 2 s. Adiabatic cross-polarization (CP) experiments were performed with 60-kHz radio-frequency field strength on ^1H and 43 kHz on ^{13}C with a CP contact time of 800 μs and a repetition time of 2.5 s for the pH 7 (512 scans) and 2 s for the pH 6 sample (32 scans). Processing and visualization of NMR spectra were performed with TOPSPIN (version 3.5; Bruker Biospin) and CcpNmr.

EPR Measurements and Data Analysis. Continuous-wave EPR measurements were performed at room temperature on a Bruker EMX X-Band (9.5 GHz) spectrometer equipped with an SHQ resonator (Bruker Biospin). Spectra were recorded at a microwave power of 1.011 mW with modulation amplitude of 0.1 mT at a modulation frequency of 100 kHz. The labeling efficiency was determined by numerical double integration of the spectra after polynomial background correction. The spin concentration was calculated with respect to a reference sample of 100 μM 4-Hydroxy-TEMPO radical (Sigma-Aldrich), indicating complete spin labeling of α-Syn. Pulse EPR measurements were performed on a home-built Q-Band (35 GHz) spectrometer with a commercial Bruker ELEXSYS E580 acquisition system, equipped with a home-built rectangular TE102 resonator (51) and a CF935 helium flow cryostat (Oxford Instruments). Distance measurements were performed using the four-pulse DEER sequence $\pi/2 - \tau_1 - \pi - \tau_1 + \tau_2 - \pi$ at the observer frequency and $2\ \tau_1 + t - \pi$ at the pump frequency where t is the time incremented in steps of 8 ns. Delays were set to $\tau_1 = 400$ ns and $\tau_2 = 2{,}000$ ns. A delay $\tau_3 = 280$ ns passed between the first observer π pulse and the initial time of the pump pulse, corresponding to a start of the time axis at $t = \tau_3 - \tau_1 = -120$ ns. Measurements were performed at 50 K with pulse lengths of 12 ns for all pulses, phase cycling the first pulse by 180° and a shot repetition time of 4 ms. The pump pulse was placed at the maximum of the nitroxide spectrum and observer pulses were placed at a frequency offset of 150 MHz. Nuclear modulation averaging was performed in eight steps of 4 ns. Experimental data were analyzed using DeerAnalysis2019 (52). Background decay was corrected using DEERNet (generic) (53) after time traces were cropped to remove overlap artifacts. Distance distributions in a range of 1.5 to 8 nm were obtained by Tikhonov regularization.

Negative-Stain EM. α-Syn fibrils from ThT aggregation kinetics (3% seed fibrils, 84-h incubation, pH 7) were diluted with NMR buffer. Five-microliter aliquots were added to glow-discharged carbon-coated copper grids for 1 min. Grids were blotted and washed twice with drops of water before staining with 2% (wt/vol) uranyl acetate for 15 s. EM images were acquired on a FEI Morgagni 268 transmission electron microscope operated at 100 kV.

Data Availability. All study data are included in the article and/or *SI Appendix*.

ACKNOWLEDGMENTS. This work was supported by the Swiss National Science Foundation (Sinergia grant CRSII5_177195/1). T.W. acknowledges support by ETH Career SEED-69 16-1 and ETH Research Grant ETH-43 17-2.

1. M. G. Spillantini *et al*., Alpha-synuclein in Lewy bodies. *Nature* **388**, 839–840 (1997).
2. M. G. Spillantini, M. Goedert, The α-synucleinopathies: Parkinson's disease, dementia with Lewy bodies, and multiple system atrophy. *Ann. N. Y. Acad. Sci.* **920**, 16–27 (2000).
3. R. Krüger *et al*., Ala30Pro mutation in the gene encoding alpha-synuclein in Parkinson's disease. *Nat. Genet.* **18**, 106–108 (1998).
4. J. J. Zarranz *et al*., The new mutation, E46K, of alpha-synuclein causes Parkinson and Lewy body dementia. *Ann. Neurol.* **55**, 164–173 (2004).
5. S. Appel-Cresswell *et al*., Alpha-synuclein p.H50Q, a novel pathogenic mutation for Parkinson's disease. *Mov. Disord.* **28**, 811–813 (2013).
6. S. Lesage *et al*.; French Parkinson's Disease Genetics Study Group, G51D α-synuclein mutation causes a novel parkinsonian-pyramidal syndrome. *Ann. Neurol.* **73**, 459–471 (2013).
7. P. Pasanen *et al*., Novel α-synuclein mutation A53E associated with atypical multiple system atrophy and Parkinson's disease-type pathology. *Neurobiol. Aging* **35**, 2180.e1–2180.e5 (2014).
8. M. H. Polymeropoulos *et al*., Mutation in the alpha-synuclein gene identified in families with Parkinson's disease. *Science* **276**, 2045–2047 (1997).
9. P. Ibáñez *et al*., Causal relation between α-synuclein gene duplication and familial Parkinson's disease. *Lancet* **364**, 1169–1171 (2004).
10. A. B. Singleton *et al*., alpha-Synuclein locus triplication causes Parkinson's disease. *Science* **302**, 841 (2003).
11. F.-X. Theillet *et al*., Structural disorder of monomeric α-synuclein persists in mammalian cells. *Nature* **530**, 45–50 (2016).
12. D. Eliezer, E. Kutluay, R. Bussell Jr, G. Browne, Conformational properties of α-synuclein in its free and lipid-associated states. *J. Mol. Biol.* **307**, 1061–1073 (2001).
13. C. R. Bodner, C. M. Dobson, A. Bax, Multiple tight phospholipid-binding modes of α-synuclein revealed by solution NMR spectroscopy. *J. Mol. Biol.* **390**, 775–790 (2009).
14. R. Bussell, Jr, D. Eliezer, A structural and functional role for 11-mer repeats in α-synuclein and other exchangeable lipid binding proteins. *J. Mol. Biol.* **329**, 763–778 (2003).
15. B. I. Giasson, I. V. Murray, J. Q. Trojanowski, V. M. Lee, A hydrophobic stretch of 12 amino acid residues in the middle of alpha-synuclein is essential for filament assembly. *J. Biol. Chem.* **276**, 2380–2386 (2001).
16. H.-T. Li, H.-N. Du, L. Tang, J. Hu, H.-Y. Hu, Structural transformation and aggregation of human alpha-synuclein in trifluoroethanol: Non-amyloid component sequence is essential and beta-sheet formation is prerequisite to aggregation. *Biopolymers* **64**, 221–226 (2002).
17. H. Heise *et al*., Molecular-level secondary structure, polymorphism, and dynamics of full-length α-synuclein fibrils studied by solid-state NMR. *Proc. Natl. Acad. Sci. U.S.A.* **102**, 15871–15876 (2005).
18. L. Bousset *et al*., Structural and functional characterization of two alpha-synuclein strains. *Nat. Commun.* **4**, 2575 (2013).
19. M. D. Tuttle *et al*., Solid-state NMR structure of a pathogenic fibril of full-length human α-synuclein. *Nat. Struct. Mol. Biol.* **23**, 409–415 (2016).
20. M. Vilar *et al*., The fold of alpha-synuclein fibrils. *Proc. Natl. Acad. Sci. U.S.A.* **105**, 8637–8642 (2008).
21. B. Li *et al*., Cryo-EM of full-length α-synuclein reveals fibril polymorphs with a common structural kernel. *Nat. Commun.* **9**, 3609 (2018).
22. R. Guerrero-Ferreira *et al*., Cryo-EM structure of alpha-synuclein fibrils. *eLife* **7**, e36402 (2018).
23. W. Peelaerts *et al*., α-Synuclein strains cause distinct synucleinopathies after local and systemic administration. *Nature* **522**, 340–344 (2015).
24. F. Chiti, C. M. Dobson, Protein misfolding, functional amyloid, and human disease. *Annu. Rev. Biochem.* **75**, 333–366 (2006).
25. A. K. Buell *et al*., Solution conditions determine the relative importance of nucleation and growth processes in α-synuclein aggregation. *Proc. Natl. Acad. Sci. U.S.A.* **111**, 7671–7676 (2014).
26. V. N. Uversky, J. Li, A. L. Fink, Evidence for a partially folded intermediate in alpha-synuclein fibril formation. *J. Biol. Chem.* **276**, 10737–10744 (2001).
27. L. A. Munishkina, E. M. Cooper, V. N. Uversky, A. L. Fink, The effect of macromolecular crowding on protein aggregation and amyloid fibril formation. *J. Mol. Recognit.* **17**, 456–464 (2004).
28. S. Campioni *et al*., The presence of an air-water interface affects formation and elongation of α-Synuclein fibrils. *J. Am. Chem. Soc.* **136**, 2866–2875 (2014).
29. C. Galvagnion *et al*., Lipid vesicles trigger α-synuclein aggregation by stimulating primary nucleation. *Nat. Chem. Biol.* **11**, 229–234 (2015).
30. R. Gaspar *et al*., Secondary nucleation of monomers on fibril surface dominates α-synuclein aggregation and provides autocatalytic amyloid amplification. *Q. Rev. Biophys.* **50**, e6 (2017).
31. F. A. Ferrone, J. Hofrichter, H. R. Sunshine, W. A. Eaton, Kinetic studies on photolysis-induced gelation of sickle cell hemoglobin suggest a new mechanism. *Biophys. J.* **32**, 361–380 (1980).
32. L. Giehm, D. E. Otzen, Strategies to increase the reproducibility of protein fibrillization in plate reader assays. *Anal. Biochem.* **400**, 270–281 (2010).
33. G. Meisl *et al*., Molecular mechanisms of protein aggregation from global fitting of kinetic models. *Nat. Protoc.* **11**, 252–272 (2016).
34. W. Hoyer *et al*., Dependence of alpha-synuclein aggregate morphology on solution conditions. *J. Mol. Biol.* **322**, 383–393 (2002).
35. C. W. Bertoncini *et al*., Release of long-range tertiary interactions potentiates aggregation of natively unstructured alpha-synuclein. *Proc. Natl. Acad. Sci. U.S.A.* **102**, 1430–1435 (2005).
36. M. Schweighauser *et al*., Structures of α-synuclein filaments from multiple system atrophy. *Nature* **585**, 464–469 (2020).
37. W. Hoyer, D. Cherny, V. Subramaniam, T. M. Jovin, Impact of the acidic C-terminal region comprising amino acids 109-140 on α-synuclein aggregation in vitro. *Biochemistry* **43**, 16233–16242 (2004).
38. J. A. Rodriguez *et al*., Structure of the toxic core of α-synuclein from invisible crystals. *Nature* **525**, 486–490 (2015).
39. R. L. Croke, S. M. Patil, J. Quevreaux, D. A. Kendall, A. T. Alexandrescu, NMR determination of pKa values in α-synuclein. *Protein Sci.* **20**, 256–269 (2011).
40. X. Yang, B. Wang, C. L. Hoop, J. K. Williams, J. Baum, Probing acetylated-α-synuclein monomer–aggregate complexes by NMR elucidates mechanism of fibril seeding. *bioRxiv* [Preprint] (2020). https://www.biorxiv.org/content/10.1101/2020.08.17.254508v1 (Accessed 25 September 2020).
41. I. M. van der Wateren, T. P. J. Knowles, A. K. Buell, C. M. Dobson, C. Galvagnion, C-terminal truncation of α-synuclein promotes amyloid fibril amplification at physiological pH. *Chem. Sci. (Camb.)* **9**, 5506–5516 (2018).
42. N. C. Prymaczok, R. Riek, J. Gerez, More than a rumor spreads in Parkinson's disease. *Front. Hum. Neurosci.* **10**, 608 (2016).
43. X. Hu *et al*., Amyloid seeds formed by cellular uptake, concentration, and aggregation of the amyloid-beta peptide. *Proc. Natl. Acad. Sci. U.S.A.* **106**, 20324–20329 (2009).
44. M. Johnson, A. T. Coulton, M. A. Geeves, D. P. Mulvihill, Targeted amino-terminal acetylation of recombinant proteins in E. coli. *PLoS One* **5**, e15801 (2010).
45. P. Kumar, I. M. J. Segers-Nolten, N. Schilderink, V. Subramaniam, M. Huber, Parkinson's protein α-Synuclein binds efficiently and with a novel conformation to two natural membrane mimics. *PLoS One* **10**, e0142795 (2015).
46. P. Schanda, E. Kupce, B. Brutscher, SOFAST-HMQC experiments for recording two-dimensional heteronuclear correlation spectra of proteins within a few seconds. *J. Biomol. NMR* **33**, 199–211 (2005).
47. P. Kumari, L. Frey, A. Sobol, N.-A. Lakomek, R. Riek, ^{15}N transverse relaxation measurements for the characterization of μs-ms dynamics are deteriorated by the deuterium isotope effect on ^{15}N resulting from solvent exchange. *J. Biomol. NMR* **72**, 125–137 (2018).
48. S. W. Fesik, E. R. P. Zuiderweg, Heteronuclear three-dimensional NMR spectroscopy of isotopically labelled biological macromolecules. *Q. Rev. Biophys.* **23**, 97–131 (1990).
49. T. Wiegand *et al*., CONFINE-MAS: A magic-angle spinning NMR probe that confines the sample in case of a rotor explosion. *J. Biomol. NMR* **72**, 171–177 (2018).
50. C. R. Morcombe, K. W. Zilm, Chemical shift referencing in MAS solid state NMR. *J. Magn. Reson.* **162**, 479–486 (2003).
51. Y. Polyhach *et al*., High sensitivity and versatility of the DEER experiment on nitroxide radical pairs at Q-band frequencies. *Phys. Chem. Chem. Phys.* **14**, 10762–10773 (2012).
52. G. Jeschke *et al*., DeerAnalysis2006—A comprehensive software package for analyzing pulsed ELDOR data. *Appl. Magn. Reson.* **30**, 473–498 (2006).
53. S. G. Worswick, J. A. Spencer, G. Jeschke, I. Kuprov, Deep neural network processing of DEER data. *Sci. Adv.* **4**, eaat5218 (2018).